

Supplementary Information

Enhanced Schottky effect via 2D-2D CoP/g-C₃N₄ interface for prominent boosting of photocatalytic H₂ evolution

Xiao-jing Wang,^{ab} Xiao Tian,^a Ying-jie Sun,^a Jia-yu Zhu,^a Fa-tang Li,^{*a} Hui-ying Mu,^a and Jun Zhao^a

^a College of Science, Hebei University of Science and Technology, Shijiazhuang, 050018, China

^b State Key Laboratory of Inorganic Synthesis and Preparative Chemistry, College of Chemistry, Jilin University, Changchun 130012, China

Experimental section

Synthesis procedure

Synthesis of pristine g-C₃N₄ and CoP nanosheets

Pristine g-C₃N₄ was fabricated by the thermal polymerization of urea according to the report.¹ Briefly, 20g of urea was added into a closed ceramic crucible with a lid to decrease sublimation of urea. The crucible was calcined at 550°C with the furnace heating rate at 10 °C/min for 3 h. After the crucible was cooled to room temperature in the furnace, the light-yellow product was collected and ground into powder for further used.

For preparation of CoP nanosheets, Co(OH)₂ nanosheets were fabricated firstly according to the reference.² Firstly, Co(OAc)₂ was dissolved in 5 mL deionized water under magnetic stirring. Then, carboxymethyl cellulose (CMC, 10mL, 1g/L) was added, and the mixture was stirred for 30min. After that, 10mL diluted ammonia solution (10 wt%) was added dropwise into the rapidly stirred solution and stirred for 1h. The obtained solution was transferred to a 40mL Teflon-lined auto clave, which was sealed and heated at 80 °C for 12h. The precipitate was collected by centrifuging, washed with deionized water and ethanol for several times and dried in freeze drier. Afterwards, 50mg of obtained Co(OH)₂ nanosheets were put on the upper layer of the ceramic steam box and 350mg of NaH₂PO₂ solid was added in the ceramic steam box, and then the ceramic steam box was put in a quartz tube of the tube furnace. Subsequently the samples were maintained at 300 °C for 2h with a heating rate of 5 °C/min in a flowing 30 mL/min Ar atmosphere. Following cooling to room temperature in continuous Ar flow, the obtained black solid powders were collected and ground into powder for further experiment.

Synthesis of CoP/g-C₃N₄ composites

The schematic illustration for fabrication of two-dimensional CoP/g-C₃N₄ composites is shown in Fig. S1. Firstly, a calculated amount of Co(OAc)₂ was dissolved in 5 mL deionized water under magnetic stirring. Then, 10mL CMC solution (1g/L) was added, and the mixture was stirred for 30min. After that, pristine g-C₃N₄ was ultrasonic dispersed in the mixture of CMC and Co(OAc)₂ solution for 1h. Finally, 10mL diluted ammonia solution (10 wt%) was added dropwise into the solution and stirred for another 1h. The following procedure was similar to the above mentioned for the CoP synthesis. The obtained samples were denoted as x%CoP/g-C₃N₄, where x is the wt% of CoP in the composite calculated from the initial concentration of Co(OAc)₂. For comparison, the zero-dimensional/two-dimensional CoP/g-C₃N₄ composite with 2% CoP was prepared using a similar procedure by replacing of CMC solution with pure water, which was denoted as 2%DCoP/g-C₃N₄.

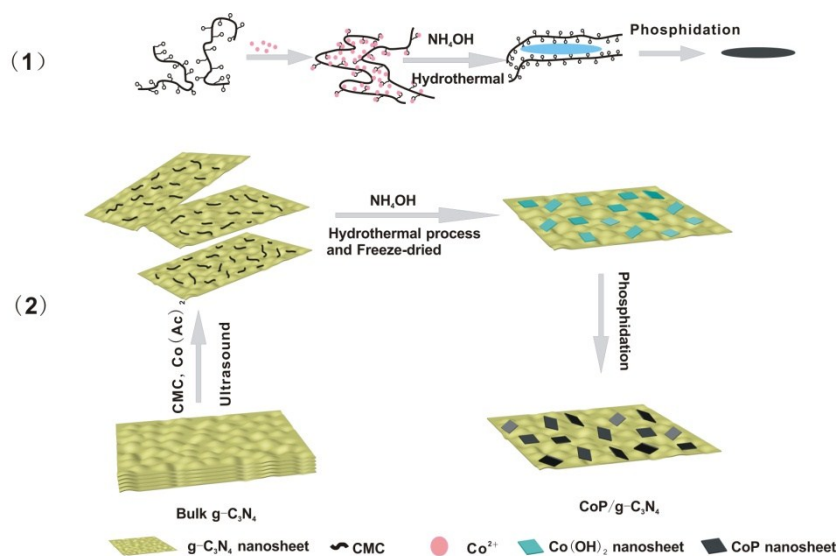


Fig. S1. Schematic illustration for the fabrication of two-dimensional CoP/g-C₃N₄ composite

Characterization

X-ray powder diffraction (XRD) patterns were measured by Rigaku D/MAX 2500 X-ray diffractometer with CuK α radiation. The morphology and microstructure of the samples were recorded by Scanning Electron Microscope (SEM) on HITACHI S-4800 and Transmission Electron Microscopy (TEM) on JEOL JEM-2100. X-ray photoelectron spectroscopy (XPS) measurements were carried out on PHI 1600 ESCA XPS system. All binding energies were referenced to the C1s peak at 284.6 eV. The Brunauer-Emmett-Teller (BET) surface area was recorded on

Micromeritics Tristar II 3020 apparatus. The photoluminescence (PL) measurements and UV-visible (UV-vis) diffuse reflectance spectra (DRS) were acquired on Edinburgh FS5 fluorescence spectrophotometer and Thermo Fisher Evolution 220 spectrophotometer, respectively. Time-resolved fluorescence decay spectra were measured on FLS980 fluorescence spectrophotometer (Edinburgh Instruments, Edinburgh, Britain) at room temperature. Electron spin resonance (ESR) measurements were analyzed on a Bruker EMX-8/2.7 X-band ESR spectrometer operating in the X-band at 9.86 GHz and 2.005 mW. The work function of the samples was measured on SKP5050 Scanning Kelvin Probe. The Inductive Coupled Plasma-Atomic Emission Spectrometry (ICP-AES) analysis was measured by ICP Optical Spectrum Instrument on ICAP 6300 (Thermo), and Microwave Digestion System was used to pretreat the as-prepared samples.

The polarization curves, photocurrent measurements and Nyquist plots were conducted on Chenhua CHI660E electrochemical analyzer using a three-electrode system in 0.5 M Na₂SO₄ electrolyte. For photocurrent measurements, Xe lamp (300 W, PerfectLight, with 400 nm cut-off filter) was employed as the light source. The working electrode was prepared as follows: 50 mg of catalyst was dispersed into a mixture of 0.98 mL of absolute ethanol and 20 μ L of 5% Nafion solution, and then, the mixture was sonicated for 30 min. After that, 20 μ L of the catalyst slurry was spread on cleaned 1.5 cm \times 1.0 cm fluoride-tin oxide (FTO) glass electrode. A platinum wire and Ag/AgCl electrode were used as the counter electrode and reference electrode, respectively.

Photocatalytic H₂ production activity

The photocatalytic hydrogen evolution was measured in a side irradiation Pyrex cell with magnetic stirring. A Xe-lamp (300 W, PerfectLight, with 400 nm cut-off filter) was used as the visible-light source. Typically, 50 mg of photocatalyst powders were added into 100mL of aqueous solution containing of 25 ml triethanolamine (TEOA) as the sacrificial reagents. The reaction temperature was controlled to be 20 °C. The hydrogen production was analyzed by a gas chromatograph (GC) equipped on a Techcomp GC7900 every 1 h, with a thermal conductive detector(TCD) and argon was chosen as the carrier gas.

The apparent quantum efficiency (AQE) was tested under the same reaction condition except the cut-off filter of the Xe-lamp was change to a $\lambda=420\pm 20$ nm band-pass filter. The average light intensity was 7.4mW/cm² and the irradiation area was 19.6 cm². The irradiation time is 10800s. The AQE was calculated based on Eq(1).³

$$\begin{aligned} \text{AQE}(\%) &= \frac{\text{Number of reacted electrons}}{\text{Number of incident photons}} \times 100\% \\ &= \frac{\text{Number of evolved H}_2 \text{ molecules} \times 2}{\text{Number of incident photons}} \times 100\% \end{aligned} \quad (1)$$

Computational details

We base our simulations on spin-polarized DFT calculations within the projected augmented wave (PAW) scheme as implemented in Vienna ab initio Simulation Package (VASP)⁴⁻⁸. During all calculations, the kinetic energy cutoff of 500eV was used, and the convergence criteria for energy and force are 10^{-5} eV and 0.01 eV/Å, respectively. For the calculation of charge density difference, we placed a 13x15 Å slab of g-C₃N₄ on the periodically repeated CoP (100) surface modeled with 5x3 super cells which is about six atomic layers. During the relaxation, we fixed four bottom layers of the six layers, and considered the dipole correction. A vacuum separation of about 20 Å is employed in order to eliminate interactions between two adjacent unit cell. The first Brillouin Zone is sampled with a k-point mesh of 9x14x8 within the Monkhorst–Packing scheme⁹ for geometry optimization of bulk CoP, and the optimized lattice constants of bulk CoP are $a = 5.06 \text{ \AA}$, $b = 3.27 \text{ \AA}$ and $c = 5.54 \text{ \AA}$, excellently consistent with the experimental values.¹⁰

The surface energy was examined which defined as follows:

$$E_{surf} = \frac{E_{slab} - E_{bulk}}{2A}$$

Where E_{slab} and E_{bulk} are the total energy of the slab and the bulk CoP with the same number of CoP formula units as in the slab, respectively. A is the surface area. The results show that the P-terminated surface is more stable than that of Co terminated, agreeing well with previous theoretical results.¹⁰

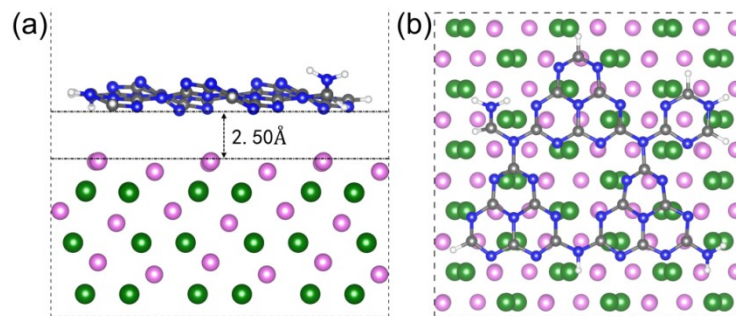


Fig. S2. The side (a) and top views (b) of the optimized structure of CoP(100)\g-C₃N₄ composites. The interlayer distance is about 2.50 Å. Green, pink, blue, grey and white spheres represent Co, P, N, C, and H atoms, respectively.

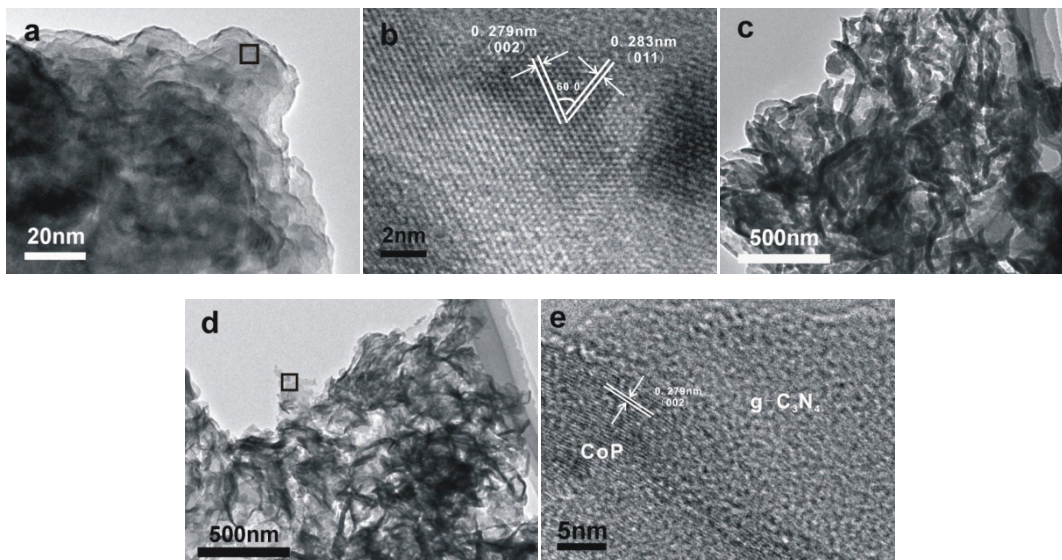


Fig. S3. (a)TEM images of bare CoP, (b) HRTEM images of of the selected box in (a), (c) TEM images of g-C₃N₄, (d) TEM images of 2%CoP/CN composite and and (e) HRTEM images of the selected box in (d)

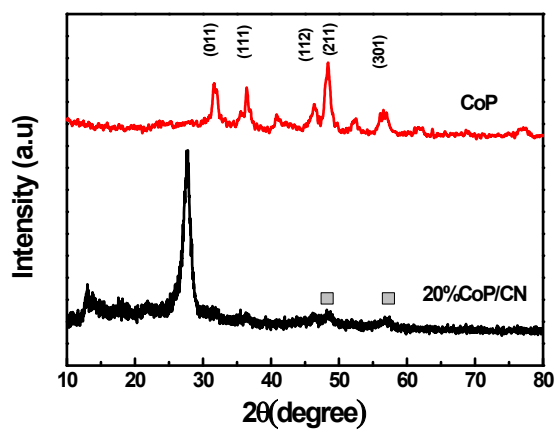


Fig. S4. XRD patterns of bare CoP and 20% CoP/g-C₃N₄ composite

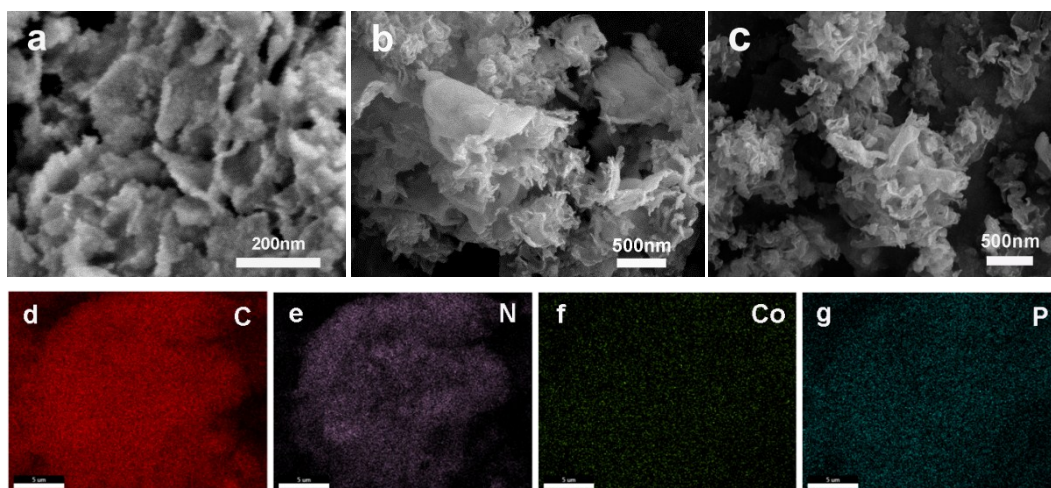


Fig. S5. SEM images of (a) bare CoP, (b) g-C₃N₄, (c) 2%CoP/CN composite and SEM mapping 2%CoP/CN composite (d)C, (e)N, (f)Co, (g)P

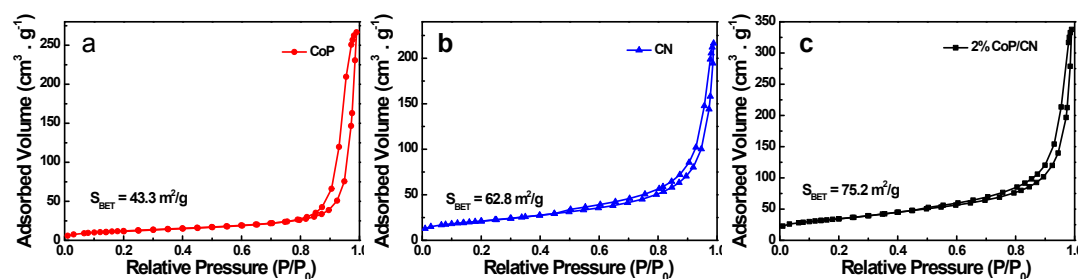


Fig. S6. Nitrogen adsorption-desorption isotherms of (a) bare CoP, (b) g-C₃N₄ and (c) 2%CoP/CN composite

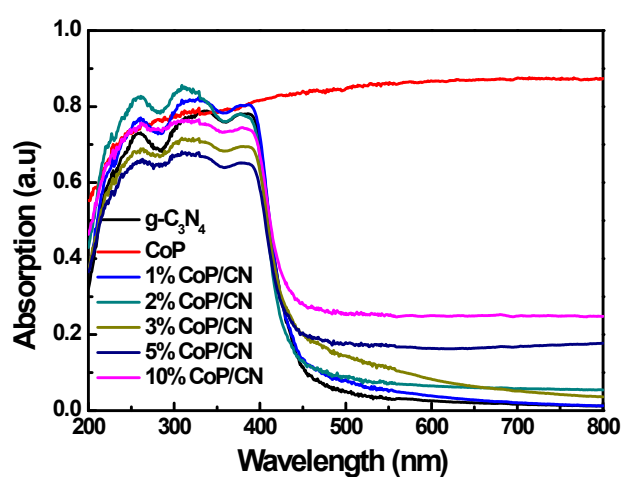


Fig. S7. UV-Vis diffuse reflectance spectra of g-C₃N₄ and xCoP/CN composites

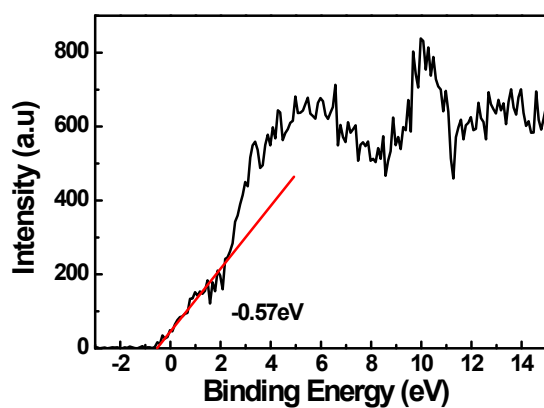


Fig. S8. XPS valence band spectra of CoP

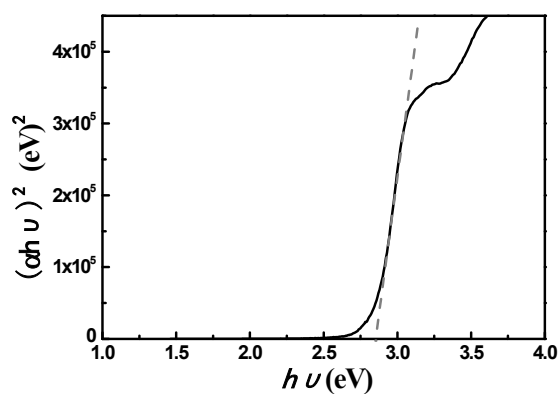


Fig. S9. The band gap of bare $g\text{-C}_3\text{N}_4$ derived from the Tauc plots using the Kubelka-munk function

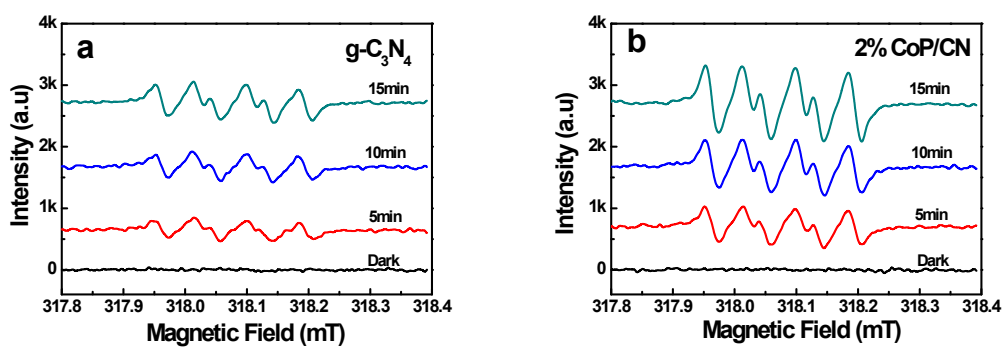


Fig. S10. ESR spectra of DMPO- $\bullet\text{O}_2^-$ adducts before and after visible light irradiated different time (a) $g\text{-C}_3\text{N}_4$ (b) 2%CoP/CN.

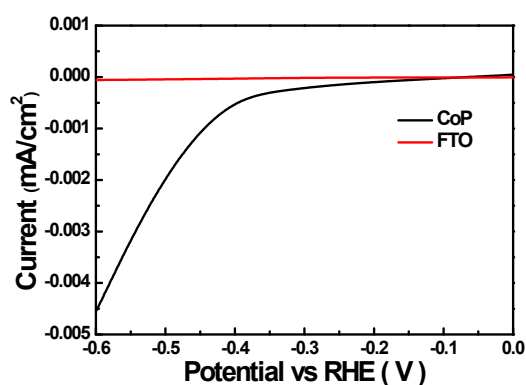


Fig. S11. Polarization curves of CoP and FTO

Table. S1. The Co and P contents of the as prepared samples detected by ICP-AES.

Sample	Co content /wt%	P content /wt%	Co/P molar ratio
1%CoP/CN	0.69	0.45	0.81
2%CoP/CN	1.21	0.86	0.74
3%CoP/CN	1.92	1.33	0.76
5%CoP/CN	3.04	2.30	0.73
10%CoP/CN	6.22	4.53	0.72
20%CoP/CN	13.05	8.66	0.79

References

1. P. Niu, L. Zhang, G. Liu and H. M. Cheng, *Adv. Funct. Mater.*, 2012, **22**, 4763–4770.
2. L. Wang, C. Song, Y. Shi, L. Dang, Y. Jin, H. Jiang, Q. Lu and F. Gao, *Chem. Eur. J.*, 2016, **22**, 5575–5582.
3. K. Chang, M. Li, T. Wang, S. Ouyang, P. Li, L. Liu and J.H. Ye, *Adv. Energy Mater.*, 2015, **5**, 1402279.
4. P. E. Blöchl, *Phys. Rev. B*, 1994, **50**, 17953.
5. J.J. Mortensen, L.B. Hansen and K.W. Jacobsen, *Phys. Rev. B*, 2005, **71**, 035109.
6. J.P. Perdew, K. Burke and M. Ernzerhof, *Phys. Rev. Lett.*, 1996, **77**, 3865–3868.

7. G. Kresse and J. Furthmüller, *Comput. Mater. Sci.*, 1996, **6**, 15–50.
8. P. Käckell, J. Furthmüller, F. Bechstedt, G. Kresse and J. Hafner, *Phys. Rev. B*, 1996, **54**, 10304.
9. H. J. Monkhorst and J. D. Pack, *Phys. Rev. B*, 1976, **13**, 5188.
10. C. Zhang, Y. Huang, Y.F. Yu, J.F. Zhang, S.F. Zhuo and B. Zhang, *Chem. Sci.*, 2017, **8**, 2769–2775.